Multi-objective optimization of a hydro-wind-photovoltaic power complementary plant with vibration absorber strategy

Hualin Xiong[a,b], Mònica Egusquiza[c], Poul Alberg Østergaard[d], Juan I. Pérez-Díaz[e], Eduard Egusquiza[c], Edoardo Patelli[f], Beibei Xu*[a,b,g,h], Hongjiang Duan[h], Xingqi Luo[g], Diyi Chen*[a,b]

[a]*Key Laboratory of Agricultural Soil and Water Engineering in Arid and Semiarid Areas, Ministry of Education, Northwest A & F University, Shaanxi Yangling 712100, P. R. China*
[b]*Institute of Water Resources and Hydropower Research, Northwest A&F University, Shaanxi Yangling 712100, P. R. China*
[c]*Center for Industrial Diagnostics (CDIF), Polytechnic University of Catalonia (UPC), Barcelona, Spain*
[d]*Department of Planning, Aalborg University, Rendsburggade 14, 9000, Aalborg, Denmark*
[e]*Department of Hydraulic, Energy, and Environmental Engineering, ETSICCP, Universidad Politécnica de Madrid (UPM), Madrid, Spain*
[f]*Department of civil and environmental engineering, University of Strathclyde, U.K.*
[g]*State Key Laboratory of Eco-hydraulics in Northwest Arid Region, Xi'an University of Technology, Xi'an, 71065, P.R. China*
[h]*Powerchina Northwest Engineering Corporation Limited, Limited, Xi'an, 710065, P.R. China*

Corresponding author: Beibei Xu, Diyi Chen
Mailing Address: Institute of Water Resources and Hydropower Research, Northwest A&F University, Shaanxi Yangling 712100, China
Telephones: 086-181-6198-0277
E-mail: xubeibei0413@163.com; diyichen@nwafu.edu.cn

Abstract: Hydropower has the advantages of quickly responding to load variability, which overcome the unpredictability and instability variability of solar and wind power. Therefore, such power generation can be combined into a hydro-wind-photovoltaic complementary plant (HWPCP). However, hydropower units running in partial load are prone to vibration, and operation in or crossing vibration zones may affect the operation and ultimately cause structural damage and affect the power plant. The problem of avoiding running hydropower units in the vibration zones is effectively addressed in this study. This is achieved by adopting a vibration absorber strategy to determine the rational power distribution scheme of hydropower units. A multi-objective optimization is performed to maximizing power generation, minimizing output power fluctuation and minimizing deviation between power generation and planned output. The power distribution strategies of hydropower units under 12 scenarios, composed of different inflow and weather conditions are analyzed. The results obtained indicate that the vibration absorber strategy effectively avoids the operation of hydropower units in the vibration zones, and ensures the operation of hydropower units in the non-vibration zone for more than 99.31% of the operation time. This study contributes to the identification of the relationship between conflicting objectives, and provides operational strategies for the safe and stable operation of hydropower units.

Keywords: Coordinated optimized operation; Multi-objective optimization; Hydro-wind-photovoltaic; Vibration zone

1. Introduction

With the continuous growth of renewable energy exploitation such as wind and photovoltaic (PV) power, curtailment has become increasingly prominent in China. From 2010 to 2016, 150.4 million MWh of renewable electricity generation was curtailed in China, a total energy loss equivalent to 48 million tons of coal consumption or 134 million tons of CO_2 emissions [1]. Due to the fast start and flexible regulation characteristics of hydropower units, the coordinated operation of hydropower, PV and wind power is considered as an important way to solve this problem. Hydro-wind systems [2, 3], hydro-PV systems [4, 5] and hydro-wind-PV systems [6, 7] have been proposed. However, the continuous adaptation to the load to compensate the variability of the wind and solar systems causes the hydropower units to operating in or crossing the vibration zone more frequently. This has the potentiality to compromise the safe and stable operation of hydropower units and is therefore relevant research topic.

Existing studies about hydro-wind-PV complementary plants (HWPCP) have shown the potentiality of the plants of improving the power quality [8], smoothing wind and PV power output fluctuations [9], optimizing short-term power grid dispatch [10], and reducing the total operating cost of renewable energy [11]. The hydropower units are a key component of HWPCP for controlling the stability of the plant's power output. To balance the influence of wind and photoelectric power, the hydropower unit need to adjust output power more frequently than in a hydropower plant. Such behavior can produce significant vibration problems such as vortex rope in the draft tube and pressure pulsations, which may affect the safe and stable operation of the hydropower station [12].

There is a lack of strategies to ensure the safe and stable operation of hydropower units in HWPCP, and more attention is needed on the hydrology and power dispatching [13]. Xu et al. [14] concluded that hydropower units frequently operated under non-rated conditions exhibits unpredicted fatigue failures and that these failures show strong correlation to the wind and solar power production. Kern et al. [15] found that reservoir releases made at rated hydro-turbine capacity became shorter and more frequent and increased sub-daily variation in downstream flows. Wang et al. [16] proposed a novel operation strategy (referred to as adaptive simultaneous peak regulation strategy) to determine the day-ahead production plan of hydro-thermal-wind-photovoltaic interconnected power systems. Yang et al. [17] formulated a two-layer nested model for the day-ahead generation scheduling of a HWPCP. The above research articles studied the regulating effect of hydropower units in HWPCP, but did not consider the influence of the vibration zone of hydropower unit, even though this is an important element in the overall study of HWPCP.

Various optimization strategies have been used to determine the hydrology regulation and generation schedule of HWPCP. With respect to the hydrology regulation, Ming et al. [18] proposed a two-layer nested optimization framework with cuckoo search algorithm (CS), and result showed that water consumption decreased by 1.5% and 1.0% in deterministic and stochastic operation scenarios. Cheng et al. [19] presented a multi-step progressive optimality algorithm (MSPOA) for optimizing the operation of complex hydropower systems to meet complex demands. Regarding to the generation schedule, in [20] the moth-flame optimization (MFO) algorithm was used to determine the optimal dispatch of a hydro-thermal-wind (HTW) system. The ant colony optimization (ACO) was used to

estimate the optimal design of a HWPCP with an electrolysis plant, a hydrogen storage tank and a fuel cell unit [21]. Mehdinejad et al. [22] proposed a hybrid approach based on imperialist competitive algorithm (ICA) and particle swarm optimization (PSO) to find the solution of optimal reactive power dispatch (ORPD) of power systems. The above research papers mainly focus on the application of advanced optimization algorithms to hydrology regulation and power dispatch, but ignore the influence of the stable operation of hydropower units on the dispatching process.

From the reviewed, the following research gaps are identified:

1. Understanding the relationship between the hydrology regulation and power dispatching of HWPCP, while this relationship is affected by the adjusting quality of hydropower unit, it could bring a different perspective and expand the current understanding.
2. There is limited research into the combination of hydropower unit vibration zones and the optimization algorithms under coordinated operation.

The significance of this work lies in three main aspects, including:

•A vibration absorber strategy aimed to minimize the number of times operate at or cross the hydro units vibration zones is proposed to ensure the safe and stable operation of hydropower units in HWPCP.

•The influence of reservoir inflow, planned output and weather factors on the short-term optimal operation of HWPCP is revealed.

•A short-term HWPCP multi-objective optimization model is established and solved by multi-objective particle swarm optimization algorithm (MOPSO) and non-dominated sorting genetic algorithm II.

The structure of this paper is as follows. In Section 2, the vibration absorber strategy is introduced. In section 3, the multi-objective model of HWPCP is established, and MOPSO and NSGA-II are introduced. The case is analyzed and discussed in Section 4. Finally, in Section 5, the main results and contributions are summarized.

2. Vibration absorber strategy for hydropower units

In a HWPCP, hydropower units are required to operate under off-design conditions in order to balance the power fluctuation of wind and photovoltaic power (see Fig. 1a). In machines such as Francis turbines, different problems may arise when working outside of its Best Efficiency Point (BEP), such as cavitation or fatigue damage [23]. One of the most critical issues is the emergence of the cavitating vortex rope, which appears at the outlet of the runner (see Fig. 1b). This phenomenon can occur either when the turbine is operating below (part-load vortex rope) or above its BEP (overload vortex rope). While the latter is more dangerous than the former, both cases lead to large instabilities, power swing and harmful vibrations in the machine, which may end up causing catastrophic damage. Therefore, to ensure the safety of the unit and to avoid a reduction of its Remaining Useful Life (RUL) it is indispensable to avoid or reduce the amount of time operating under these conditions.

The vibration absorber strategy presented in this study is used to reduce the number of times the units operate in or pass through the regarded vibration zones by distributing the output between different hydropower units. The flow chart of vibration absorber strategy is shown in Fig. 2. The specific process includes:

Step 1: Define the vibration zone and non-vibration zone for the case in question. The hydraulic pulsation under different water head and output power for hydro-turbine units are measured based on the standard Code for Field Measurement of Vibration and Pulsation in Hydraulic Machines (turbines,

storage pump and pump-turbine) (GB/T-17189-2017) [24]. Experimental measurements show that the operation zone of Francis units can be divided into vibration zones and non-vibration zones, as shown in Fig. 3. These zones can be identified in each turbine with different methods [25-27]. A sketch of a general turbine is indicated in Fig. 4.

Step 2: Calculate the difference P^{DI}_t between the grid load and the output power of the HWPCP. First, obtain the output power of the wind generation system P^{W}_t, the output power of the PV system P^{S}_t and the grid load demand P^{L}_t in the period t. Second, assuming the output power of the hydropower station is maintained as the last period value $P^{AS}_t=P^{H}_{t-1}$. Finally, the difference is obtained, i.e. $P^{DI}_t=P^{L}_t-P^{W}_t-P^{S}_t-P^{AH}_t$.

Step 3: Evaluate the operation mode of the HWPCP.

(1) The assumed sum output power $P^{AS}_t=P^{AH}_t+P^{S}_t+P^{W}_t$ of HWPCP is equal to the demand of the grid load P^{L}_t, meaning that the output state of the hydropower station in the previous period is maintained $P^{H}_t=P^{AH}_t$.

(2) The assumed sum output power P^{AS}_t is less than the grid load demand P^{L}_t.

Case 1: all the hydropower units are already at the maximum output state $P^{H}_{i,t-1}=P^{max}_i$, therefore the hydropower output power is maintained $P^{H}_t=P^{AH}_t$.

Case 2: there are hydropower units with output power less than P^{max}_i, their output power is increased to meet the equation $P^{H}_t=P^{DI}_t+P^{H}_{t-1}$.

(3) The assumed sum output power P^{AS}_t is greater than the grid load demand P^{L}_t.

Case 1: all hydropower units are already at the minimum output state $P^{H}_{i,t-1}=P^{min}_i$, the output power of hydropower is maintained $P^{H}_t=P^{AH}_t$, and the wind power or PV output is limited.

Case 2 there are hydropower units with output power greater than P^{min}_i, their output power is decreased to meet the equation $P^{H}_t=P^{DI}_t+P^{H}_{t-1}$.

Step 4: Coordinate the output power of hydropower units. There are three principles to coordinate the output power of hydropower units.

a. Ensure the hydropower units operating in a non-vibration zone.

b. Avoid the hydropower units crossing a vibration zone when adjusting the output power.

c. When an inevitable crossing is demanded to maintain power balance, unit i# with the smallest change of output power has the higher priority to pass through the vibration zone.

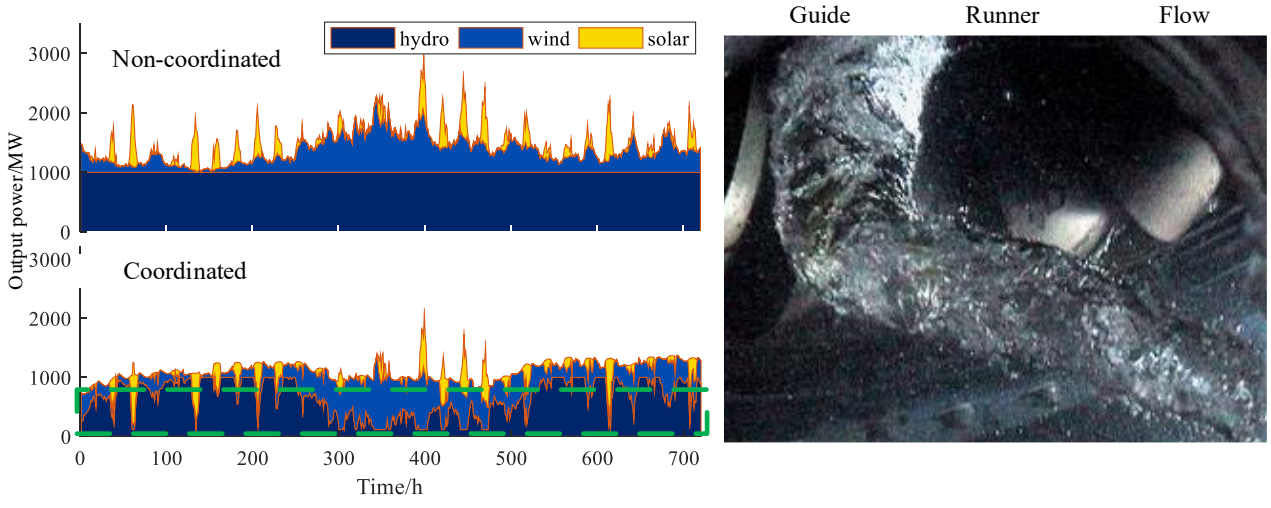

(a) Output power under non-coordinated and coordinated operating modes [28]. (b) Water flow near the hydro-turbine guide vanes under coordinated operating modes [29].

Fig. 1. Comparison of hydropower units under conventional and complementary operation modes. In Fig. 1b,

Picture of a part load vortex rope in the draft tube of a Francis turbine model. The draft tube vortex rope is generated because the flow leaving the runner rotates when the turbine operates at part load.

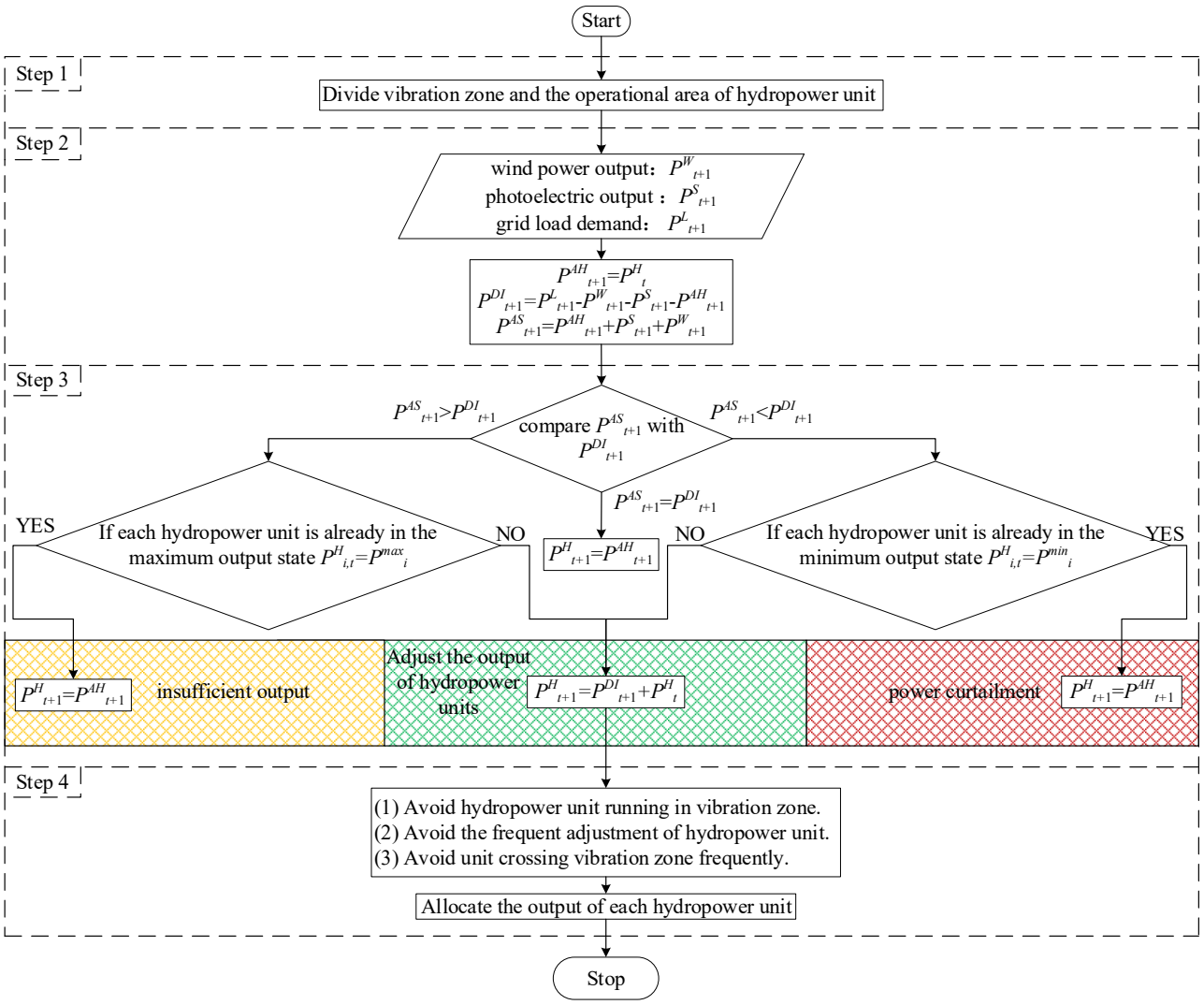

Fig. 2. Flow chart of vibration absorber strategy for the hydro-wind-PV power complementary plant.

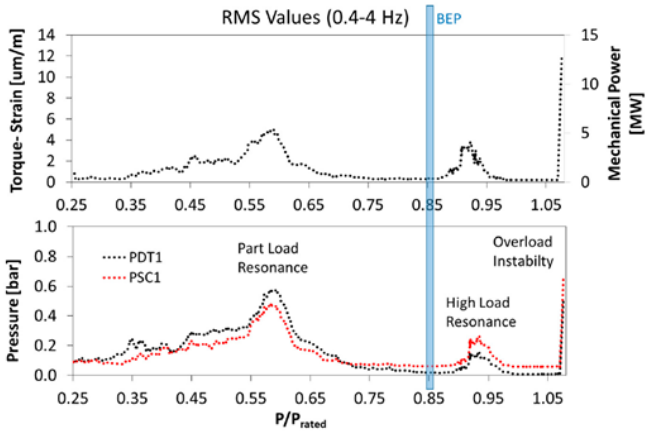

Fig 3. Zones of high vibration in the operation of a Francis turbine [30].

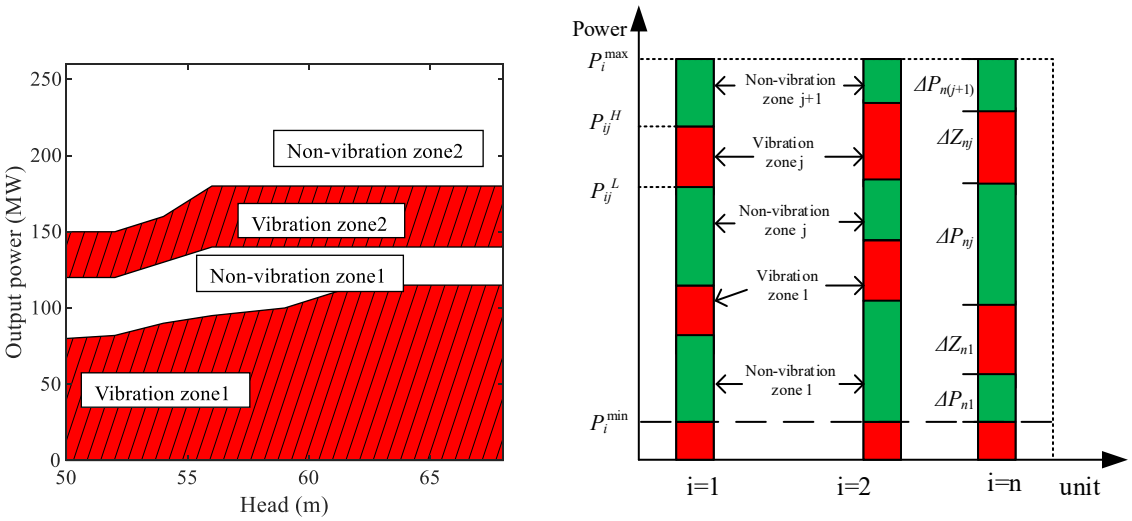

(a) The operation zone of a hydropower unit. (b) The adjustment sequence of hydropower units.

Fig. 4. Schematic diagram of hydropower units' vibration zone. Symbols $P_i^{\min}$ and $P_i^{\max}$ are the minimum and maximum output power of the i^{th} hydropower unit, respectively; P_{ij}^{H} and P_{ij}^{L} are the upper and lower limits output power of the i^{th} hydropower unit's j^{th} vibration zone, respectively; ΔP_{ij} and ΔZ_{ij} are the range of the i^{th} hydropower unit's j^{th} non-vibration zone and vibration zone, respectively.

3. Multi-objective model of HWPCP

HWPCP aims at increasing the total power generation [31], reducing the output fluctuation of wind power and PV power [32], and reducing the deviation between actual and planned power output [33], as shown in Fig. 5. From Fig. 5a, the objective of increasing the total generating capacity leads to larger power fluctuations, which affects the integration of wind power and PV power in the grid. From Fig. 5b, the hydropower generation with frequent regulation is used to balance the fluctuation of wind and PV output power, which affects the stability of hydropower units. From Fig. 5c, the objective of minimizing the deviation between actual and planned power output leads to the curtailment of wind and solar generation considering the planned output of the power grid. Obviously, these objectives are contradictory. A proper multi-objective approach is required to simultaneously consider all the objectives.

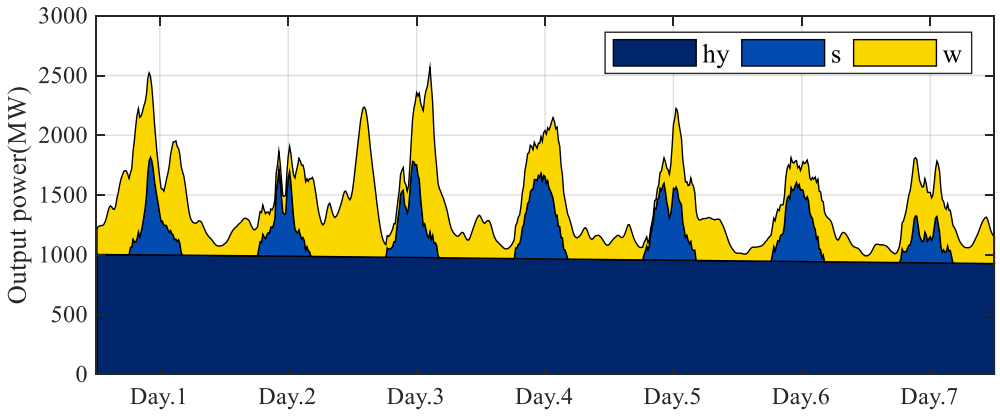

(a) Maximum the total power generation

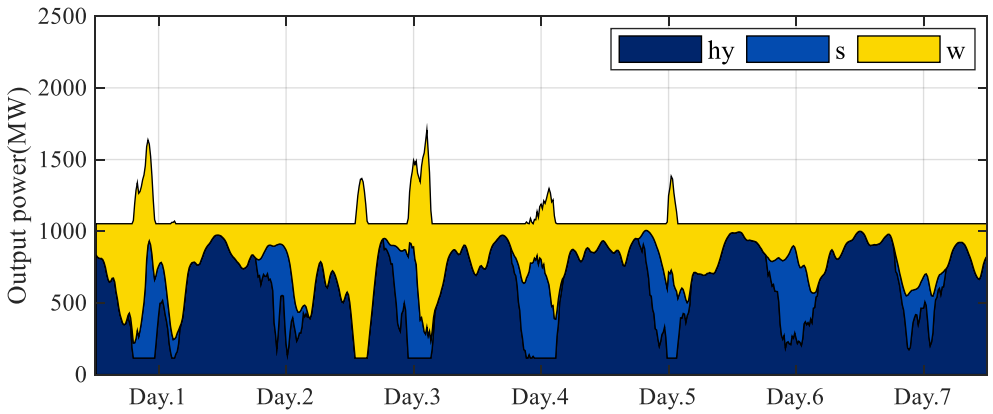

(b) Minimum the power fluctuation.

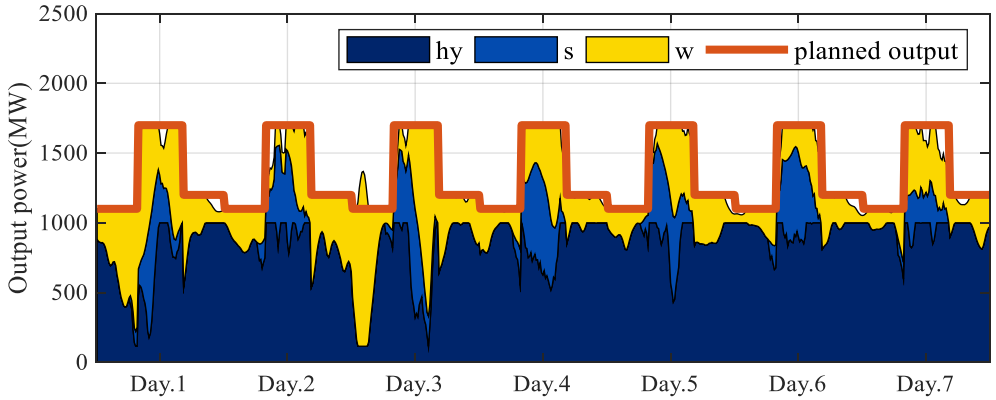

(c) Minimizing the deviation between the actual and planned power output.

Fig. 5. Multiple objectives of the hydro-wind-PV complementary plant. The block of dark blue, light blue and yellow are the hydropower, PV and wind output power of the hydro-wind-PV complementary plant, respectively. The orange line is the planned output.

Obviously, these objectives are contradictory. Thus, it is significantly to obtain the optimal coordination strategy. This section describes the objective function, the constraints and the solution algorithm.

3.1 Objective function

The three parts of the objective function are described in the following.

3.1.1 Maximizing power generation

The hydropower system output is adjusted hourly, thus a day is divided into N=24 periods. The objective function of maximizing the power generation is

$$\max\left(\sum_{t=1}^{N}\left(P_t^W + P_t^S + P_t^H\right)\times\Delta t\right). \tag{1}$$

Where $P^W{}_t$, $P^S{}_t$, and $P^H{}_t$ are the output of wind power, PV power, and hydropower in the period t, respectively; N is the total number of intervals within the time range; Δt is the time interval.

3.1.2 Minimizing output power fluctuation

The output power fluctuation of the HWPCP is reflected by Mei-Wang Fluctuation Index [34], which combines standard deviation and rotation angle. A diagram of the rotation angle is shown in Fig. 6. The objective function of minimizing output power fluctuation is

$$\min\left(\sum_{t=1}^{N}\left(\exp\left(\theta_t\right)-1\right)\times\sqrt{1/N\times\sum_{t=1}^{N}\left(P_t^T-\overline{P^T}\right)^2}\right)$$

$$\theta_t=\begin{cases}\arctan\left|k_t\right| & t=1,or,N\\ \left|\arctan k_t-\arctan k_{t-1}\right| & 1\le t\le N-1,and,k_t\times k_{t-1}\ge 0\\ \arctan\left|k_t\right|+\arctan\left|k_{t-1}\right| & 1\le t\le N-1,and,k_t\times k_{t-1}<0\end{cases}. \quad (2)$$

$$k_t=\begin{cases}\dfrac{P_{t+1}^T-P_t^T}{t_{t+1}-t_t} & 1\le t\le N-1\\ k_{N-1} & t=N\end{cases}$$

$$P_t^T=P_t^W+P_t^S+P_t^H$$

Where P^T_t is the total output power of the HWPCP in the period t. $\overline{P_t^T}$ is the mean value of P^T; θ_t is the rotation angle of the P^T_t in the period t. k_t is the gradient between P^T_t and P^T_{t+1}.

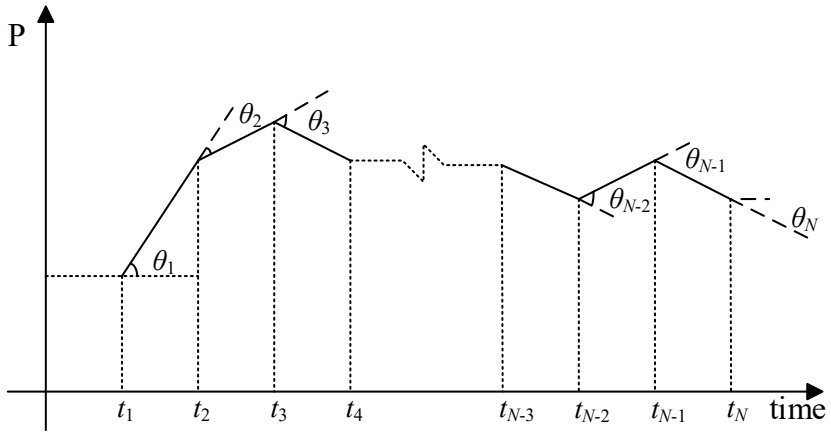

Fig. 6. Schematic diagram of the rotation angle of Mei-Wang Fluctuation Index.

3.1.3 Minimizing the deviation between actual and planned power output

From Fig. 5c, the limited regulating capacity of hydropower causes power curtailment and load shedding of the wind and PV power. Thus, minimizing the deviation between the actual and planned power output is adopted as the objective function, which is

$$\min\frac{1}{N}\left(\sum_{t=1}^{N}\left(P_t^L-P_t^T\right)^2\right)^{\frac{1}{2}}. \quad (3)$$

Where P^L_t is the planned output given by power dispatch center in the period t ; P^T_t is the total output power of the HWPCP in the period t.

3.2 Constraints

The constraints used in this model are as follows: [35]

(1) The reservoir level constraint is

$$Z^{\min H}\le Z_t^H\le Z^{\max H}. \quad (4)$$

where $Z^{\min H}$ and $Z^{\max H}$ are the minimum and maximum reservoir level, respectively; Z_t^H is the reservoir level in the period t.

(2) The reservoir capacity constraint is

$$V^{\min H} \le V_t^H \le V^{\max H}. \tag{5}$$

where $V^{\min H}$ and $V^{\max H}$ are the minimum and maximum reservoir capacity, respectively; V_t^H is the water storage of the reservoir in the period t.

(3) The discharge flow constraint is

$$Q^{\min H} \le Q_t^H \le Q^{\max H}. \tag{6}$$

where $Q^{\min H}$ and $Q^{\max H}$ are the minimum and maximum discharge flow of the reservoir, respectively; Q_t^H is the discharge flow of the reservoir in the period t.

(4) The water balance constraint is

$$V_{t+1}^H = V_t^H + \left(q_t - \sum_{i=1}^{M_1} Q_{i,t} - S_t \right) \Delta t. \tag{7}$$

where q_t is the reservoir inflow in the period t; $Q_{i,t}$ is the power generation flow of hydropower unit i# in the period t; S_t is the surplus water of the reservoir in the period t; M_1 is the number of the hydropower units; Δt is the time interval.

(5) The hydropower output constraint is

$$\begin{cases} P_{i,t}^H = A_i Q_{i,t} h_{i,t} \\ P_{i,t+1}^H - P_{i,t}^H \le \Delta P_{i,up}^H \\ P_{i,t}^H - P_{i,t+1}^H \le \Delta P_{i,down}^H \end{cases}, \tag{8}$$

where $h_{i,t} = Z_t^H - Z_t^T - h_i^l$.

where $P^H_{i,t}$ is the output of the hydropower unit i# in the period t; A_i is the output coefficient of the hydropower unit i#; $Q_{i,t}$ is the generation flow of the hydropower unit i# in the period t; $h_{i,t}$ is the water head of the hydropower unit i# in the period t; $\Delta P^H_{i,up}$ and $\Delta P^H_{i,down}$ are the upward and downward capacity of the i^{th} hydropower unit, respectively; Z^T_t is the tailwater level in the period t; h^l_i is the head loss of the i^{th} hydropower unit's conduits.

(6) The vibration zone constraint is

$$\begin{cases} P_i^{\min} \le P_{i,t}^H \le P_{i1,t}^D \left(Z_t^H \right) \\ P_{ij,t}^U \left(Z_t^H \right) \le P_{i,t}^H \le P_{i(j+1),t}^D \left(Z_t^H \right), \quad j = 1 \sim J-1. \\ P_{iJ}^U \left(Z_t^H \right) \le P_{i,t}^H \le P_i^{\max} \end{cases} \tag{9}$$

where $P_i^{\min}$ and $P_i^{\max}$ are the minimum and maximum output of the hydropower unit i#, respectively; $P^D_{ij,t}(Z_t^H)$ and $P^U_{ij,t}(Z_t^H)$ are the lower and upper limits of the i^{th} hydropower unit's j^{th} vibration zone when the reservoir level is Z_t^H, respectively.

(7) The output power of wind constraint

The output power of wind generator set is related to wind speed, blade speed and unit structure. The power curve showing the relation between wind speed and output power is shown in Fig. 7. The wind power output is [36]

$$P_{i,t}^{W}=\begin{cases}0, & when \quad V_{i,t}\le V_{cut-in}\\ \frac{1}{2}\rho A C_p V_{i,t}^{3}, & when \quad V_{cut-in}\le V_{i,t}<V_{rated}\\ 1.5, & when \quad V_{rated}\le V_{i,t}<V_{cut-out}\\ 0, & when \quad V_{cut-out}\le V_{i,t}\end{cases}, \tag{10}$$

where $\begin{cases} C_P=0.22\left(\frac{116}{\lambda_1}-0.4\beta-5\right)e^{-12.5/\lambda_1} \\ \frac{1}{\lambda_1}=\frac{1}{\lambda+0.08\beta}-\frac{0.035}{\beta^3+1} \\ \lambda=\frac{\omega_r R}{V_r}\end{cases}$.

Where $P_{i,t}^{W}$ is the output power of the i^{th} wind turbine in the period t; ρ is the density of air; A is the swept area; $V_{i,t}$ is the wind speed flowing through the i^{th} wind turbine in the period t; $V_{cut\text{-}in}$ and $V_{cut\text{-}out}$ are the cut-in and cut-out wind speed of the wind turbine, respectively; V_{rated} is the rated speed of the wind turbine; C_p is the power coefficient of the wind turbine; λ_1 is the intermediate variable; λ is the tip speed ratio; β is the pitch angle; ω_r is the rated speed of the wind turbine; R is the wind turbine rotor radius; V_r is the rated wind speed of the wind turbine.

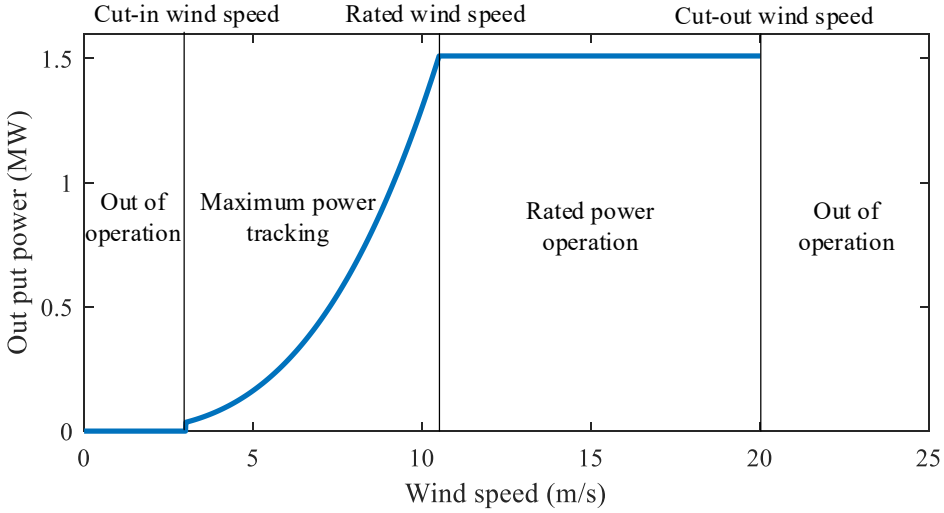

Fig. 7. Schematic power curve for wind power. When $V_{i,t}\le V_{cut\text{-}in}$ or $V_{i,t}>V_{cut\text{-}out}$, the turbine is out of operation. When $V_{cut\text{-}in}<V_{i,t}\le V_{rated}$, the turbine operates at the maximum power tracking mode. When $V_{rated}<V_{i,t}\le V_{cut\text{-}out}$, the turbine maintains the rated power output.

(8) The PV power output constraint is [37]

$$P_{i,t}^{S}=\mathrm{IC}^{PV}\times\left(\frac{R_{i,t}}{R_{stc}}\right)\times\left(1+\varphi_{PV}\times\left(T_{i,t}-T_{stc}\right)\right). \tag{11}$$

Where $P^{S}_{i,t}$ is the output of the PV system in the period t; IC^{PV} is the installed PV capacity; R_t is the intensity of solar radiation in the period t; R_{stc} is the solar radiation intensity under the standard conditions; φ_{PV} is the temperature coefficient of solar panels; T_t is the temperature in the period t; T_{stc} is the temperature under the standard conditions.

(9) The balance of output power and load demand is

$$P_t^L = P_t^H + P_t^W + P_t^S + P_t^C - P_t^A, \tag{12}$$

where $\begin{cases} P_t^H = \sum_i^{M_1} P_{i,t}^H \\ P_t^W = \sum_i^{M_2} P_{i,t}^W \\ P_t^S = \sum_i^{M_3} P_{i,t}^S \end{cases}$.

Where $P^C{}_t$ is the compensation power of other power stations in the period t when the output power of HWPCP does not meet the load demand; $P^A{}_t$ is the power curtailment of the wind and PV power in the period t. M_1, M_2 and M_3 are the number of the hydropower units, wind power units and PV panel.

3.3 Decision variables

Zhang et al. [38] proposed a multi-segment line generalization method to describe different load forms of power grids using parameterization. As shown in Fig. 8, PV power only generates electricity in the daytime. To reduce the deviation between the output power of PV and load, the three-segment line daily variation planned output $P_{1,i}$ (i=1, 2, 3) for the HWPCP is adopted as the first set of variables. The form of typical daily load curve in China is "dual-peak". So, the five-segment line daily variation planned output $P_{2,i}$ (i=1, 2, ···5) for the HWPCP is taken as the second set of variables. In this study, the difference between three-segment and five-segment line daily variation planned output modes are analysis in Section 4.4 with the same constraints formulation.

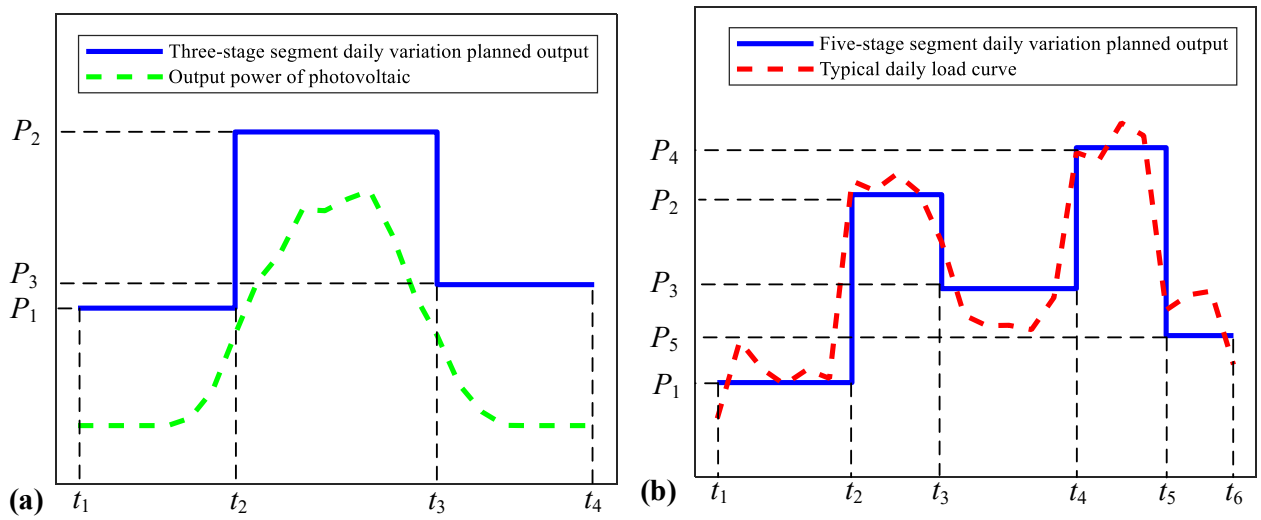

Fig. 8. Schematic diagram of the multi-segment line generalization method. (a) Three-segment line daily variation planned output. (B) Five-segment line daily variation planned output.

3.4 Multi-objective optimization algorithms

The coordinated operation of HWPCP is a multi-objective optimization problem. The multi-objective includes maximizing power generation, minimizing output power fluctuation and minimizing the deviation between actual and planned power output. The three-segment or five-segment line daily variation planned output for the HWPCP is taken as the variables. Constraints of HWPCP are nonlinearity and non-convex. Multi-objective optimization algorithms such as multi-objective particle swarm optimization algorithm (MOPSO) [39] and non-dominated sorting genetic algorithm

II (NSGA-II) [40] are widely used to solve this problem. In [41], the multi-objective particle swarm optimization algorithm (MOPSO) and the non-dominated sorting genetic algorithm II (NSGA-II) were considered to be relatively mature and versatile algorithms, thus, these two algorithms are used in this paper to solve the coordinated operation of HWPCP. To compare the characteristics of the two algorithms, the two algorithms are used in this study to obtain Pareto optimal solution sets. The flow chart of the solved process is shown in Fig. 9, and the calculation steps are described as follows for the 2 optimization algorithms used:

(a) MOPSO:

Step 1: Set the population size m=50, the maximum iterations K_{max}=1000, the inertia weight ω=0.5 and the learning factor c_1=2, c_2=2, respectively. The velocity $v_i(t)$ and position $x_i(t)$ of each particle in the population (representing the design variables) are randomly generated using uniform distributions. The output process of HWPCP is determined by the particle position.

Step 2: Calculate the fitness value (values of the objective functions) of the particle according to the fitness function. Constraints are converted into penalty terms into the objective functions. When the constraints are violated, the fitness value is punished according to the degree of damage.

Step 3: Update the individual and global extremum of the particle. If the current fitness value of the particle is superior to the individual extremum, the current particle position is denoted as the optimal position of the particle $Pbest_i(t)$. If the current fitness value of the particle is superior to the global extremum, the current particle position is denoted as the optimal position of the population $Gbest_i(t)$.

Step 4: According to the updated individual extremum and global extremum, Eq. (13) is used to update the position and velocity of the next generation particle.

$$\begin{cases} v_i(t+1) = \omega \times v_i(t) + r_1 \times c_1 \times \left(Pbest_i(t) - x_i(t) \right) + r_2 \times c_2 \times \left(Gbest(t) - x_i(t) \right) \\ x_i(t+1) = x_i(t) + v_i(t+1) \end{cases} \tag{13}$$

where r_1 and r_2 are the random values changing in the interval of [0, 1].

Step 5: Set K=K+1. If $K \leq K_{max}$, repeat the procedure from Step 2. Otherwise, output the optimal position of the population.

(b) NSGA- Ⅱ:

Step 1: Randomly generate the parent generation P_i, and each individual is assigned a non-dominant level after the non-dominant sorting.

Step 2: The first generation of offspring population Q_i is obtained by selection, crossover and mutation.

Step 3: Combine all the individuals of the parent population P_i and the offspring population Q_i into a new population R_i (R_i=$P_i \cup Q_i$). Conduct the non-dominant sorting of the combined population R_i, and calculate the local crowding degree of each individual.

Step 4: According to the non-dominant level, select individuals until the total number of individuals reaches N=50 to form a new parent population P_{i+1}. The new parent population P_{i+1} performs a new round of selection, crossover and mutation to form a new offspring population Q_{i+1}.

Step 5: Repeat steps 3 and 4 until the maximum evolutionary algebra K_{max}=1000.

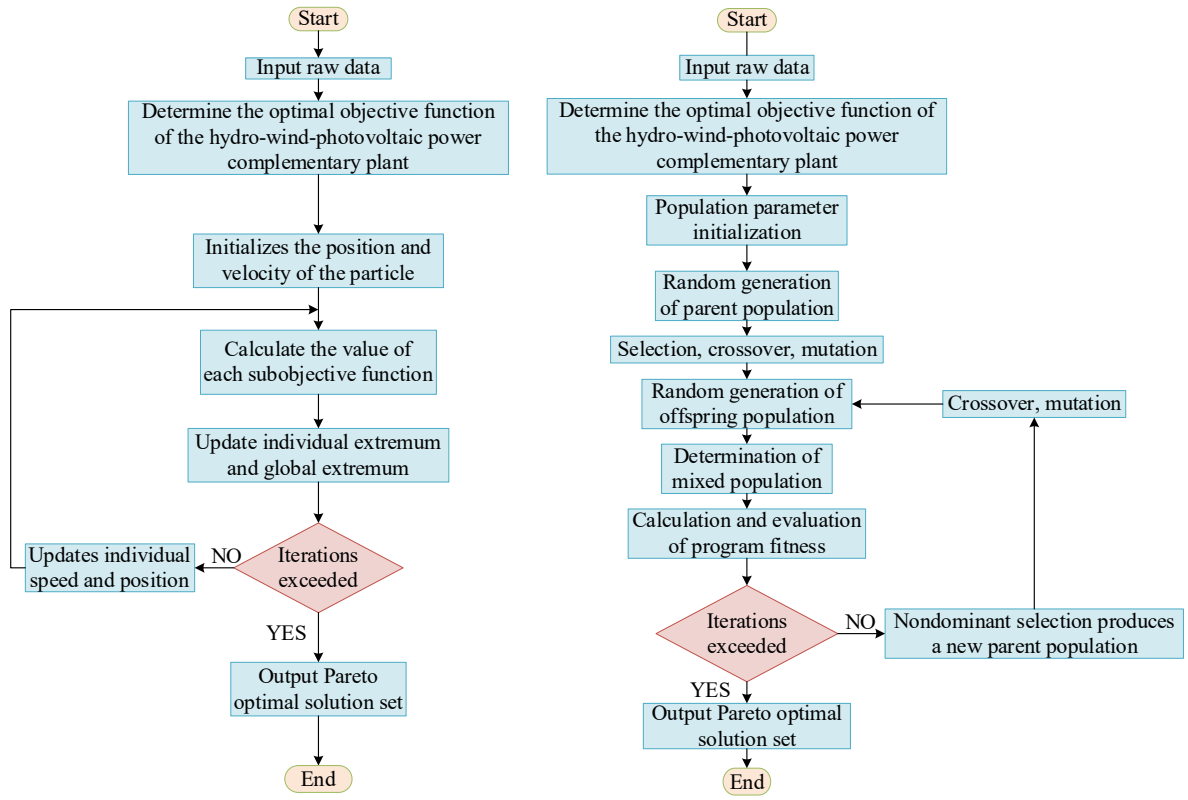

(a) The flowchart of MOPSO algorithm. (b) The flowchart of NSGA-II algorithm.

Fig. 9. The flowchart of MOPSO and NSGA-II algorithm.

4 Simulation Results

4.1 Scenario setting

Wind speed, solar intensity and reservoir inflow are uncontrollable factors in the operation of HWPCP. Therefore, 12 different scenarios with different condition of wind speed, solar intensity and reservoir inflow conditions are considered in the operation of HWPCP. The related values of different scenarios are shown in Table 1, and the variation curve of wind speed and solar intensity are shown in Fig. 10.

Table 1 The related values of different scenarios.

Scenarios	Inflow (m^3/s)	Weather	Average daily wind speed (m/s)	Average daily solar intensity (W/m^2)
1	800	rainy	7.58	87.77
2	800	cloudy	7.64	175.07
3	800	sunny	10.50	288.72
4	1200	rainy	6.09	29.91
5	1200	cloudy	7.48	100.82
6	1200	sunny	10.15	204.47
7	1600	rainy	9.36	59.69
8	1600	cloudy	9.53	106.96
9	1600	sunny	9.70	243.09
10	2000	rain	5.88	60.90
11	2000	cloudy	7.63	124.31
12	2000	sunny	12.27	298.36

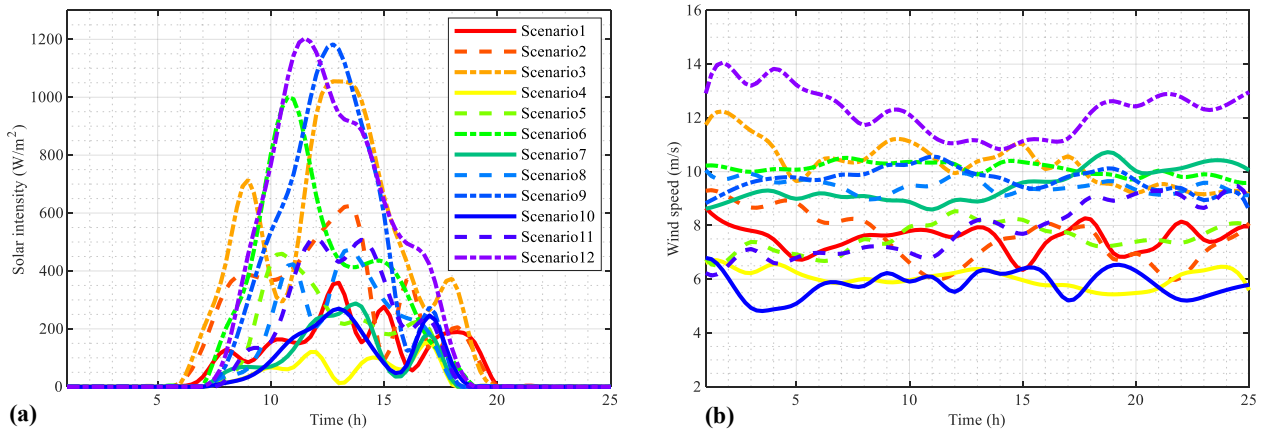

Fig. 10. The variation curve of wind speed and solar intensity within a year. (a) hourly solar intensity. (b) hourly wind speed [42].

Table 2 Operation parameters of the hydro-wind-PV power complementary plant.

Symbol	Parameter	Numerical	Unit
P_i^s	Rated power of individual solar panel	400	W
IC^{PV}	Total installed capacity of PV power generation	1200	MW
R_{stc}	Solar radiation intensity under standard conditions	1000	W/m^2
φ_{PV}	Solar panel power temperature coefficient	-0.35	%/$^\circ$C
T_{stc}	Temperature under standard conditions	25	$^\circ$C
ω_r	Rated speed of wind turbine	15.7	r/min
R	The rotor radius of wind turbine	38.5	m
V_r	Rated wind speed of wind turbine	10.5	m/s
$V_{cut\text{-}in}$	Cut-in wind speed of wind turbine	3	m/s
$V_{cut\text{-}out}$	Cut-out wind speed of wind turbine	20	m/s
ρ	Air density	1.293	kg/m^3
λ	Tip speed ratio	6.03	rad
β	Pitch angle	0.262	rad
C_p	Power coefficient of wind turbine	0.43	p.u.
P_i^W	Rated power of single wind turbine	1.5	MW
P^W	Total installed capacity of wind farm	600	MW
A	Efficiency coefficient of the hydro-turbine (HLF180AI-LJ-680)	9.01	N/m^3
Q	Rated flow of the hydro-turbine	440.4	m^3/s
H	Rated head of the hydro-turbine	63	m
P_i^H	Rated power of single hydropower unit	250	MW
P^H	Total installed capacity of hydropower unit	1000	MW
Z^I	Initial reservoir level	191.19	m
$Z^{\min H}$	Minimum reservoir level	170.00	m
$Z^{\max H}$	Maximum reservoir level	205.00	m

$V^{\min H}$	Minimum reservoir capacity	33	$10^8 m^3$
$V^{\max H}$	Maximum reservoir capacity	139	$10^8 m^3$

4.2 Coordinated operation of multiple energy sources

The multi-objective model of HWPCP is solved by MOPSO and NSGA-Ⅱ to obtain the Pareto optimal solution sets of three objective functions in 12 scenarios. In each scenario, the Pareto sets of two algorithms both contain 50 solutions. The basic parameters of HWPCP are shown in Table 2, and the obtained Pareto optimal solution sets are shown in Fig. 11.

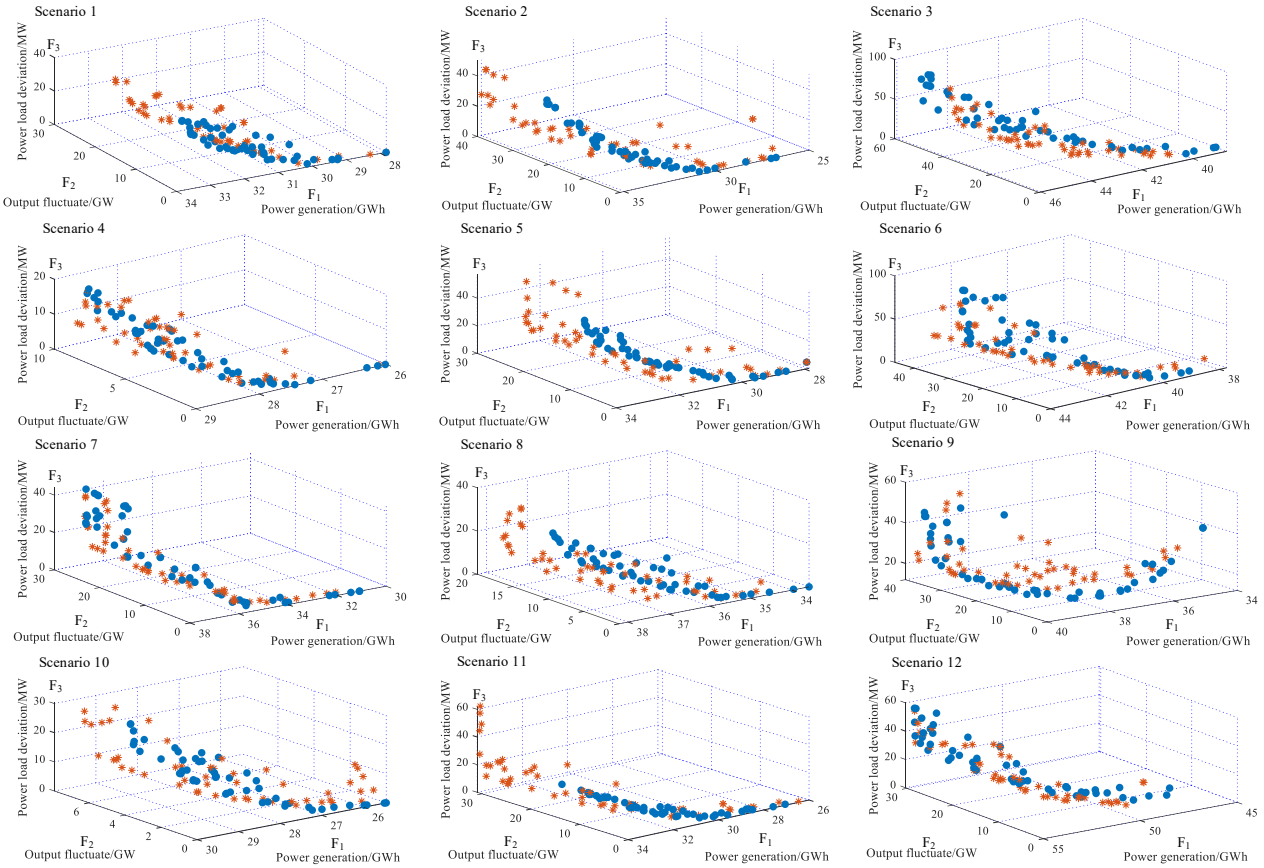

Fig. 11. Pareto optimal solution sets of three objective functions. F_1 is the power generation (GWh); F_2 is the output power fluctuation (GW); F_3 is the deviation between actual and planned power output (MW). The blue solid circle and red asterisk are the Pareto optimal solution sets solved by MOPSO and NSGA-Ⅱ, respectively.

The variables of F_1, F_2 and F_3 are the power generation, output power fluctuation, deviation between actual and planned power output, respectively. From Fig. 11, each subfigure has the same variation trend, that is one of the three objectives increases, the other two objectives decrease. The difference among every subfigure is the range of the objective functions in different scenarios. To reveal the range of the objective functions under different scenarios, the statistical results are shown in Table 3. To compare the characteristics of the two algorithms, the boxplot of Pareto solution set solved by MOPSO and NSGA-Ⅱ are shown in Fig. 12.

Table 3 Ranges of F_1, F_2 and F_3 in the considered scenarios. The blue, green and red block are the results of rainy, cloudy and sunny scenarios.

Scenarios	Inflow(m^3/s)	Weather	F_1 (GWh)			F_2 (GW)			F_3 (MW)		
			Average	Maximun	Minimum	Average	Maximun	Minimum	Average	Maximun	Minimum
1		rainy	31.3	32.5	27.8	25.2	49.5	0.0	23.9	56.2	0.0
2	800	cloudy	32.6	34.3	26.8	45.9	104.4	0.0	32.1	85.0	0.0
3		sunny	43.5	46.1	38.7	125.1	209.7	18.8	88.4	224.5	0.0
4		rainy	28.3	28.8	26.0	14.7	35.0	0.0	20.0	46.4	0.0
5	1200	cloudy	31.3	32.5	27.9	36.8	72.8	2.2	30.0	80.4	0.0
6		sunny	41.6	42.7	38.7	92.1	168.8	11.5	77.2	202.1	1.0
7		rainy	36.0	37.2	31.1	53.4	113.0	0.0	42.9	105.8	0.0
8	1600	cloudy	36.6	37.8	33.6	22.8	49.7	0.0	29.3	63.9	0.0
9		sunny	38.2	39.8	34.5	88.0	152.8	22.7	58.3	124.8	28.7
10		rainy	28.0	29.0	25.5	11.0	24.9	0.0	25.1	58.3	0.0
11	2000	cloudy	31.3	33.0	27.0	25.9	75.1	0.3	18.4	40.0	0.0
12		sunny	52.8	54.8	46.9	69.2	124.5	9.1	65.2	137.1	16.9

From Table 3, the comparison of Pareto solutions under different weather conditions shows: (1) for power generation F_1, it is always $F_{1,sunny}>F_{1,cloudy}>F_{1,rainy}$ when the inflow is same; (2) for fluctuation F_2, it is $F_{2,sunny}>F_{2,rainy}>F_{2,cloudy}$ when the inflow is 1600 m^3/s, and for other inflows it is $F_{2,sunny}>F_{2,cloudy}>F_{2,rainy}$; (3) for deviation F_3, it is $F_{3,sunny}>F_{3,rainy}>F_{3,cloudy}$ when the inflow is more than 1600 m^3/s, and for other inflows it is $F_{3,sunny}>F_{3,cloudy}>F_{3,rainy}$. The comparison of objective functions under different inflows shows:

(1) The power generation F_1 changes only slightly under the same weather scenario. (2) The average fluctuation F_2 decreases with the increase of the inflow. In conclusion, when the reservoir inflow is abundant, the hydropower units have strong regulating ability, which is effective to suppress the power fluctuation.

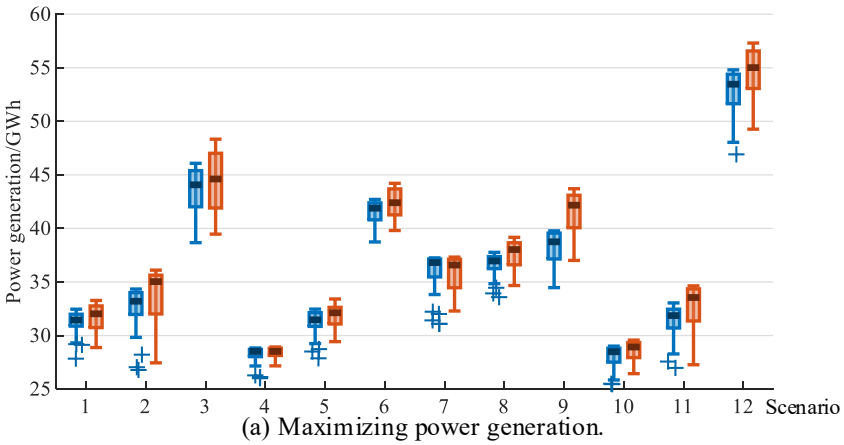

(a) Maximizing power generation.

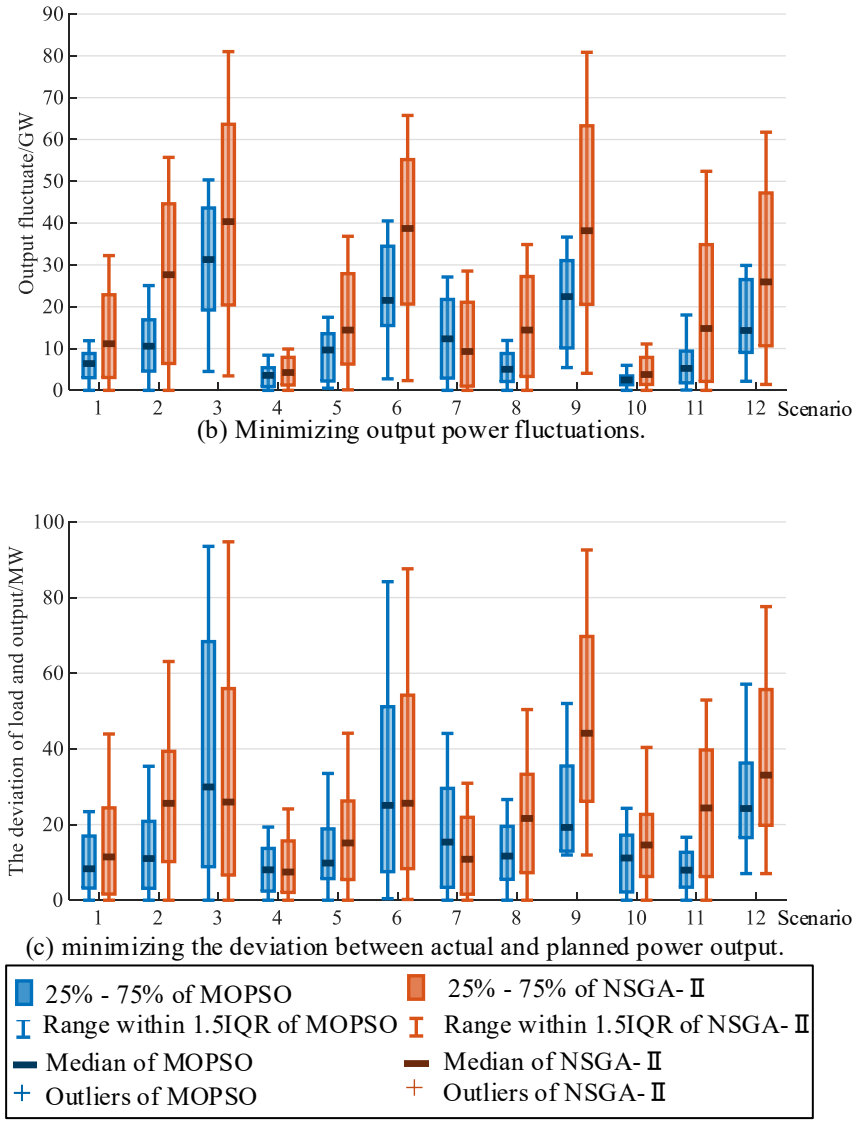

Fig. 12. Boxplot of Pareto solution set obtained by MOPSO and NSGA-Ⅱ.

From Fig. 12, the median number obtained by NSGA-Ⅱ is larger than that obtained by MOPSO in each scenario for the objective function of generation F_1. From a statistical point of view, the larger median number means the better solution set for F_1. Therefore, the NSGA-Ⅱ algorithm is more suitable for seeking the solution set of the objective function F_1. For the objection functions F_2 and F_3, the median number obtained by NSGA-Ⅱ is larger than that obtained by MOPSO in all scenarios except for Scenarios 3 and 7. The smaller median number means the better solution set for the objective functions F_2 and F_3. Hence, the MOPSO is more suitable for solving the objective functions F_2 and F_3. It is worth noting that there are outliers less than Q_1-1.5IQR for F_1 obtained by MOPSO, where Q_1 is the lower quartiles, and IQR is the interquartile range. The distance between these outliers and the optimal solution is large, which indicates that the convergence of the algorithm is poor when MOPSO is used to solve the maximum power generation F_1. In addition, the difference between the upper and lower quartiles solved by NSGA-Ⅱ algorithm is larger than that solved by MOPSO in all scenarios except for Scenarios 3 and 7. The larger difference means the wider range of the obtained solution set. Therefore, the NSGA-Ⅱ provides a wider range of solutions for decision makers, and the following analysis based on the results of the NSGA-Ⅱ.

4.3 Vibration zone of unit

To explore the operation of HWPCP after considering the vibration zone of hydropower units, Fig. 13 shows the output and the regulation of hydropower units after considering the vibration zone.

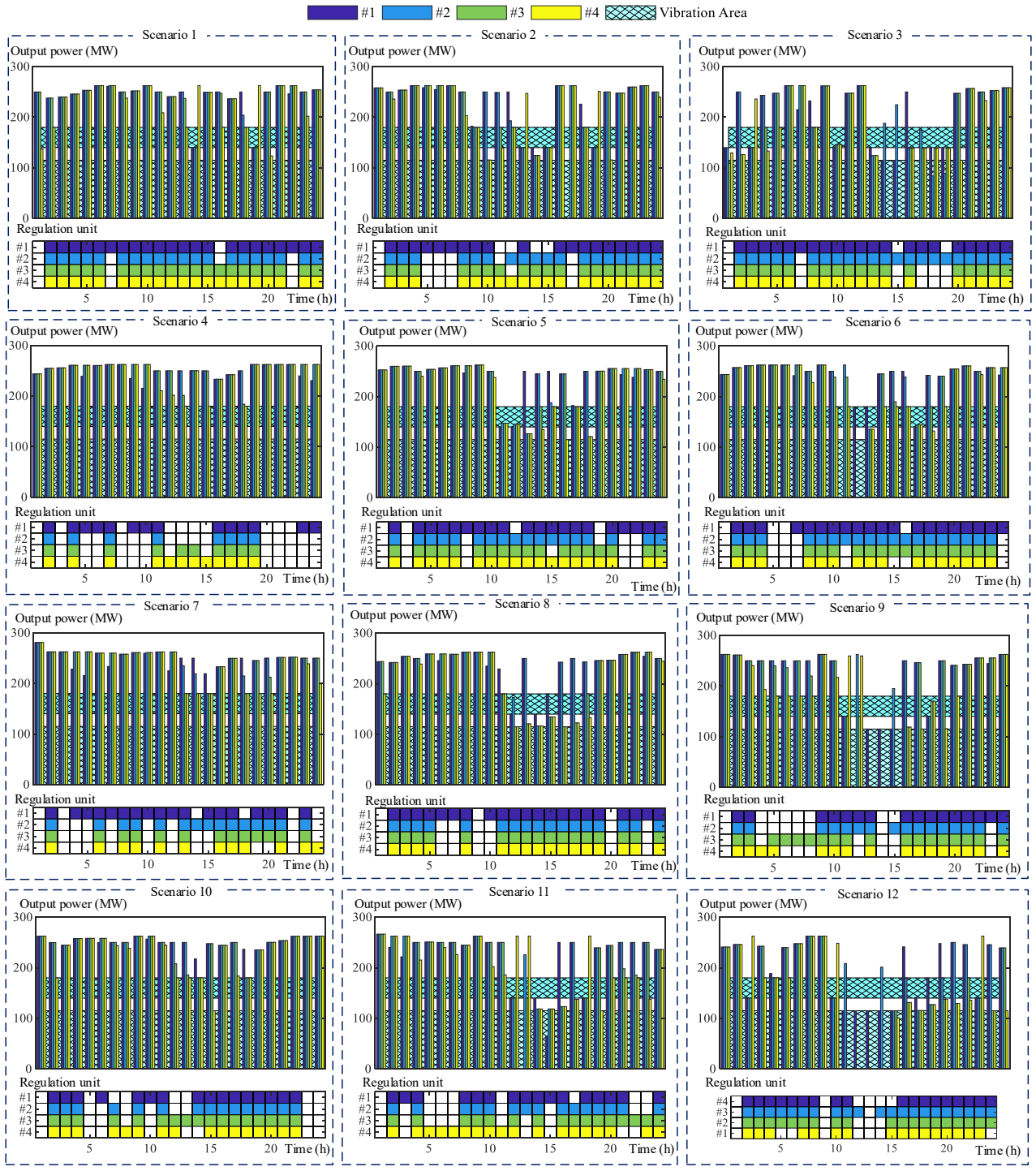

Fig. 13. The output and the regulation of hydropower units after considering the vibration zone of hydropower units.

The higher and lower diagram in each subfigure of Fig. 13 shows the output of hydropower units and whether or not the output of each units varies between two consecutive periods (colored if it varies, white if it remains constant). From Fig. 13, the vibration absorber strategy in Section 2 effectively avoids hydropower units operating in the vibration zone except scenario 11 and scenario 12. Interestingly, in scenarios 11, unit #1 still operates in the vibration zone at 15:00 to meet the balance

of load and output, otherwise, the PV or wind power is abandoned. But instead, in scenario 9, no hydropower units run in vibration zone, and power curtailment of PV and wind power happened at noon, which is shown in Fig. 14. This reflects the limitation of the vibration zone to the unit on the regulating capacity, and the opposite requirements for the safe operation of hydropower units and for the full utilization of wind and PV power in some cases.

4.4 The restriction of planned output

This subsection studies the balance between supply and demand of HWPCP under three-segment and five-segment line daily variation planned output modes. Fig.14 shows the insufficient output and the power curtailment of the HWPCP under three-segment and five-segment planned output modes.

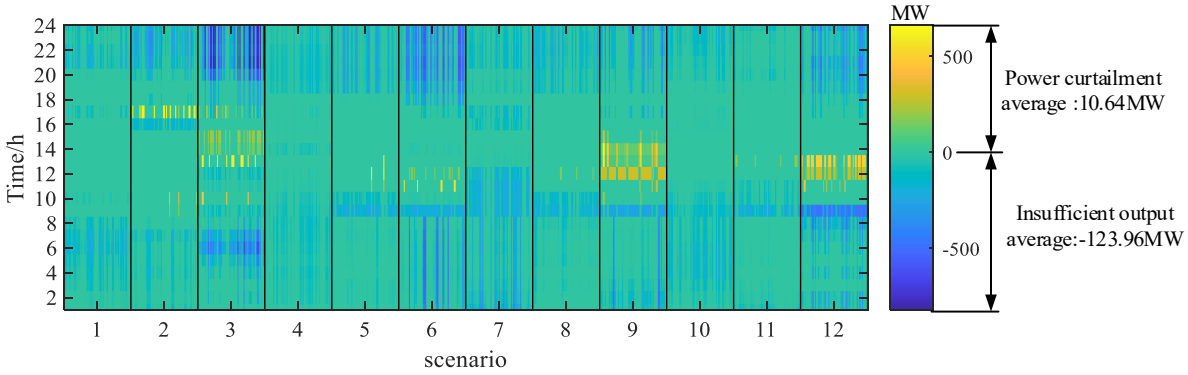

(a) The insufficient output and the curtailment of the wind and solar generation under three-segment line.

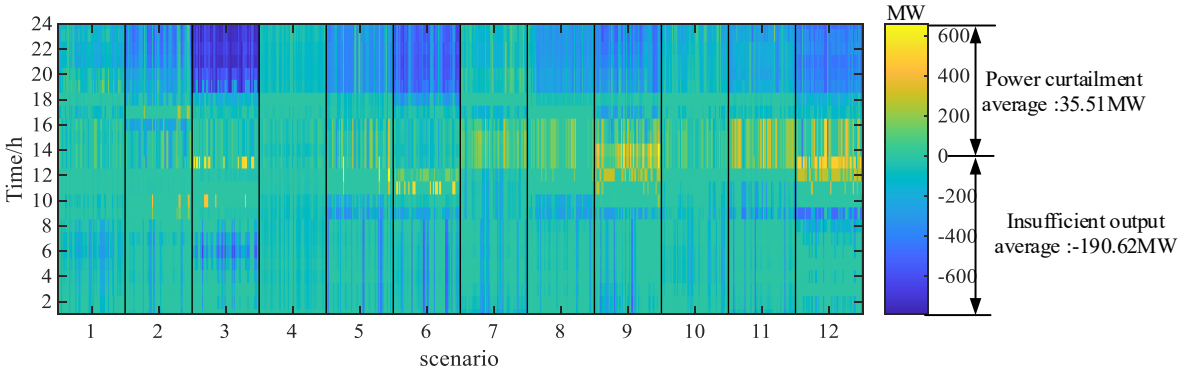

(b) The insufficient output and the curtailment of the wind and solar generation under five-segment line.

Fig. 14. The insufficient output and the power curtailment under three-segment and five-segment planned output modes. The yellow line and the blue line are the power curtailment and the insufficient output, respectively. The plot shows the 24 hours in vertical axis versus 12 scenarios in horizontal axis.

Fig.14 shows that the insufficient output and power curtailment of the five-segment output mode has a longer duration and larger shortage than three-segment output mode's, representing that the three-segment output is more suitable for HWPCP to reduce the power curtailment and insufficient output. Specially, power curtailment appears under rainy conditions (Scenarios 1, 4, 7 and 10) under the five-segment type. However, this is not the case for the three-segment type.

From Fig. 14a, under the planned output mode of the three-segment line, only Scenario 9 experience wind and solar power curtailment in the daytime, while all other scenarios do not present such power curtailment. Insufficient output is more likely to occur at night than during daytime. From Fig. 14b, under the planned output mode of the five-segment line, all scenarios exhibit power curtailment and insufficient output is present. What's more, the insufficient output and power curtailment of the five-segment output mode has a longer duration and larger shortage than three-segment output mode. In conclusion, the output mode of daily three-segment line is more suitable for hydro-wind-PV power complementary plant to reduce the power curtailment and insufficient output.

4.5 Variation of outflow and reservoir level

The outflow and reservoir level of the hydropower station have great influence on the operation of the HWPCP. In addition to power generation, the hydropower station also takes into account the

downstream flood control and irrigation, which is regulated by the outflow. The peak capacity of hydropower is insufficient if the reservoir level is too small or too large. To explore the variation rules of outflow and reservoir level in different weather and inflow, the results are shown in Fig. 15.

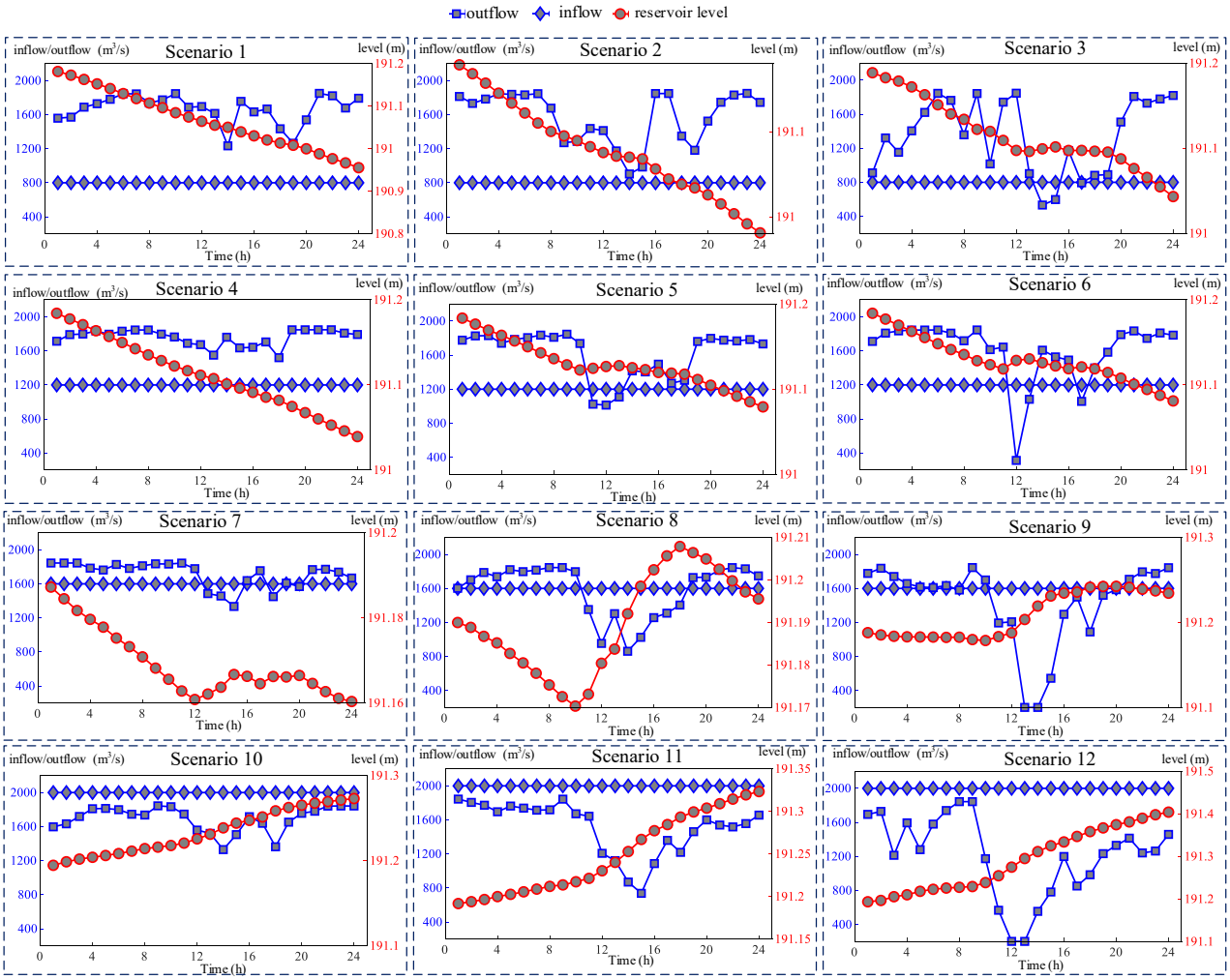

Fig. 15. Variation of outflow and reservoir level under different weather and inflow scenarios. The first, second, and third columns are the results of rainy, cloudy, and sunny days, respectively. The first, second, third and fourth row are the results of the inflow of 800 m^3/s, 1200 m^3/s, 1600 m^3/s and 2000 m^3/s, respectively.

From Fig. 15 it is possible to observe that when the inflow is less than 1200 m^3/s or more than 2000 m^3/s, the reservoir level continues to drop or rise. Thus, the inflow at 1200 m^3/s~2000 m^3/s is more appropriate for a stable reservoir level. Taking the inflow at 1600 m^3/s as an example, the deviation between the reservoir level and initial level 191.19 m at 24:00 on rainy, cloudy and sunny days is -0.030 m, +0.008 m, +0.040 m, respectively. Rainy days and sunny days obliviously effect on the water level deviation, and consecutive rainy or sunny days contribute to further increase the reservoir level deviation.

Conventional reservoirs use operation guidelines obtained as a result of the medium-term operational planning in the form of e.g. level targets at the end of the day (with corresponding thresholds). Thus, compared with the conventional hydropower station, the combination of hydrologic forecast and weather forecast has a significant impact on the operation of HWPCP. This is not only to predict the output of wind power and PV power, and also has important reference for the planned output of hydropower station.

5 Conclusions

This study has proposed a vibration absorber strategy aimed to minimize the number of times operate at or cross the hydro unit vibration zones and optimized using a multi-objective approach for HWPCP. The results obtained have shown that:

- The vibration absorber strategy effectively reduces the operation of hydropower units in the vibration zone, and hydropower units operate in the non-vibration zone for more than 99.31% of the operation time in the considered scenarios.
- Compared with the planned output model of daily five-segment, the planned output of daily three-segment increase the utilization of wind power and photoelectric resources, reduce the average wind and photoelectric power curtailment by 70.0% (10.64 MW vs 35.51 MW), and reduce the insufficient output by less than 34.9% (123.96 MW vs 190.62 MW).
- It has been shown that the MOPSO approach is more suitable for minimizing output power fluctuation F_2 and the deviation between actual and planned power output F_3. However the algorithm suffers from a poor convergence. The NSGA-Ⅱ approach is more suitable for maximizing power generation F_1, and can provide a wider range of solutions for decision makers.

Acknowledgements

This research is supported by the Fundamental Research Funds for the Northwest A&F University (No. /Z1090220172), the scientific research foundation of the Natural Science Foundation of Shaanxi Province of China (2019JLP-24), Shaanxi Science and Technology Innovation Team, and Water Conservancy Science and Technology Program of Shaanxi Province (2018slkj-9).

References:

1. Liu L, Wang Z, Wang Y, Wang J, Li S. Optimizing wind/solar combinations at finer scales to mitigate renewable energy variability in China. Renewable and Sustainable Energy Reviews. 2020;132:110151.
2. Portero, Ulises, Velazquez, Sergio, Carta, Jose A. Sizing of a wind-hydro system using a reversible hydraulic facility with seawater. A case study in the Canary Islands. Energy Conversion & Management. 2015.
3. Papaefthymiou SV, Papathanassiou SA. Optimum sizing of wind-pumped-storage hybrid power stations in island systems. RENEW ENERG. 2014;64:187-196.
4. Mahmoudimehr J, Shabani M. Optimal design of hybrid photovoltaic-hydroelectric standalone energy system for north and south of Iran - ScienceDirect. RENEW ENERG. 2018;115:238-251.
5. A JJ, B BC. Integrating photovoltaics into energy systems by using a run-off-river power plant with pondage to smooth energy exchange with the power gird - ScienceDirect. APPL ENERG. 2017;198:21-35.
6. Tang Y, Fang G, Tan Q, Wen X, Ding Z. Optimizing the sizes of wind and photovoltaic power plants integrated into a hydropower station based on power output complementarity. ENERG CONVERS MANAGE. 2020;206:112465.
7. Ma T, Yang H, Lu L, Peng J. Technical feasibility study on a standalone hybrid solar-wind system with pumped hydro storage for a remote island in Hong Kong. RENEW ENERG. 2014;69:7-15.
8. Zhang M, Xie T, Zhang C, Chen D, Shen C. Dynamic model and impact on power quality of large hydro‐photovoltaic power complementary plant. INT J ENERG RES. 2019;43.
9. Liu B, Lund JR, Liao S, Jin X, Liu L, Cheng C. Optimal power peak shaving using hydropower to complement wind and solar power uncertainty. Energy Conversion & Management. 2020;209:112621-112628.
10. Wang F, Xie Y, Xu J. Reliable-economical equilibrium based short-term scheduling towards hybrid hydro-photovoltaic generation systems: Case study from China. APPL ENERG. 2019;253.
11. Bhattacharya B, Chakraborty N, Mandal KK. A cost‐optimized power management strategy for combined wind thermal–pumped hydro generation considering wind power uncertainty. INT T ELECTR ENERGY. 2019;29.
12. Li XB, Binama M, Su WT, Cai WH, Li FC. Runner blade number influencing RPT runner flow characteristics under off-design conditions. RENEW ENERG. 2020;152:876-891.

13. Lund PD, Lindgren J, Mikkola J, Salpakari J. Review of energy system flexibility measures to enable high levels of variable renewable electricity. Renewable and Sustainable Energy Reviews. 2015;45:785-807.
14. Xu B, Chen D, Venkateshkumar M, Xiao Y, Yue Y, Xing Y, et al. Modeling a pumped storage hydropower integrated to a hybrid power system with solar-wind power and its stability analysis. APPL ENERG. 2019;248:446-462.
15. Kern JD, Patino-Echeverri D, Characklis GW. The impacts of wind power integration on sub-daily variation in river flows downstream of hydroelectric dams. ENVIRON SCI TECHNOL. 2014;48:9844.
16. Xuebin W, Jianxia C, Xuejiao M, Yimin W. Short-term hydro-thermal-wind-photovoltaic complementary operation of interconnected power systems. APPL ENERG. 2018;229:945-962.
17. Yang Y, Zhou J, Liu G, Mo L, He F. Multi-plan formulation of hydropower generation considering uncertainty of wind power. APPL ENERG. 2020;260.
18. Bo M, Pan L, Shenglian G, Lei C, Yanlai Z, Shida G, et al. Robust hydroelectric unit commitment considering integration of large-scale photovoltaic power: A case study in China. APPL ENERG. 2018;228:1341-1352.
19. Cheng C, Shen J, Wu X, Chau KW. Short-Term Hydroscheduling with Discrepant Objectives Using Multi-Step Progressive Optimality Algorithm†. JAWRA Journal of the American Water Resources Association. 2012.
20. Hazra S, Roy PK. Optimal dispatch using moth‐flame optimization for hydro‐thermal‐wind scheduling problem. INT T ELECTR ENERGY. 2020;30:n/a-n/a.
21. Menshsari A, Ghiamy M, Mohammad M, Mousavi MMM, Bagal HA. Optimal design of hybrid water-wind-solar system based on hydrogen storage and evaluation of reliability index of system using ant colony algorithm. International Journal of Sciences: Basic and Applied Research (IJSBAR). 2013;4:3582-3600.
22. Radosavljevic J, Jevtic M. Solution of Optimal Reactive Power Dispatch by a Hybrid GSA-SQP Algorithm. ELEKTRON ELEKTROTECH. 2016;22.
23. Trivedi C, Gandhi B, Cervantes MJ. Effect of transients on Francis turbine runner life: a review. J HYDRAUL RES. 2013;51:121-132.
24. General Administration Of Quality Supervision IAQO, Committee CNSA. Code for field measurement of vibrations and pulsations in hydraulic machines（turbines, storage pumps and pump-turbines）. Beijing 2017. p.
25. Valentín, Presas, Valero, Egusquiza. Detection of Hydraulic Phenomena in Francis Turbines with Different Sensors. SENSORS-BASEL. 2019;19:4053.
26. Valentin D, Presas A, Bossio M, Egusquiza M, Valero C. Feasibility to Detect Natural Frequencies of Hydraulic Turbines under Operation Using Strain Gauges. SENSORS-BASEL. 2017;18:821.
27. Zhao W, Egusquiza M, Valero C, Valentín D, Egusquiza E. On the Use of Artificial Neural Networks for Condition Monitoring of Pump-Turbines with Extended Operation. MEASUREMENT. 2020;163:107952.
28. Wang X, Virguez E, Kern J, Chen L, Wang H. Integrating wind, photovoltaic, and large hydropower during the reservoir refilling period. ENERG CONVERS MANAGE. 2019;198.
29. Trivedi C, Gandhi B, Cervantes MJ. Effect of transients on Francis turbine runner life: a review. J HYDRAUL RES. 2013;51:121-132.
30. David V, Alexandre P, Eduard E, Carme V, Mònica E, Matias B. Power Swing Generated in Francis Turbines by Part Load and Overload Instabilities. ENERGIES. 2017;10:2124.
31. Jiang Z, Song P, Liao X. Optimization of Year-End Water Level of Multi-Year Regulating Reservoir in Cascade Hydropower System Considering the Inflow Frequency Difference. ENERGIES. 2020;13:5345.
32. Zhang X, Ma G, Huang W, Chen S, Zhang S. Short-Term Optimal Operation of a Wind-PV-Hydro Complementary Installation: Yalong River, Sichuan Province, China. ENERGIES. 2018;11:868.
33. Shi J, Wang L, Lee WJ, Cheng X, Zong X. Hybrid Energy Storage System (HESS) optimization enabling very short-term wind power generation scheduling based on output feature extraction. APPL ENERG. 2019;256:113911-113915.
34. Xianxun W, Yadong M, Hao C, Xiangyu C. A New Fluctuation Index: Characteristics and Application to Hydro-

Wind Systems. ENERGIES. 2016;9.

35. Wang X, Mei Y, Kong Y, Lin Y, Wang H. Improved multi-objective model and analysis of the coordinated operation of a hydro-wind-photovoltaic system. ENERGY. 2017;134:813-839.

36. Slootweg JG, Polinder H, Kling WL, "Dynamic modelling of a wind turbine with doubly fed induction generator," in Power Engineering Society Summer Meeting, (2001).

37. Ming B, Liu P, Guo S, Zhang X, Feng M, Wang X. Optimizing utility-scale photovoltaic power generation for integration into a hydropower reservoir by incorporating long- and short-term operational decisions. APPL ENERG. 2017;204:432-445.

38. Zhang Y, Ma C, Lian J, Pang X, Qiao Y, Chaima E. Optimal photovoltaic capacity of large-scale hydro-photovoltaic complementary systems considering electricity delivery demand and reservoir characteristics. ENERG CONVERS MANAGE. 2019;195:597-608.

39. Coello Coello CA, Lechuga MS, "MOPSO: a proposal for multiple objective particle swarm optimization,", (IEEE, 2002), pp. 1051-1056.

40. Deb K, Pratap A, Agarwal S, Meyarivan T. A fast and elitist multi-objective genetic algorithm: NSGAII. IEEE T EVOLUT COMPUT. 2002;6.

41. Lian J, Zhang Y, Ma C, Yang Y, Chaima E. A review on recent sizing methodologies of hybrid renewable energy systems. ENERG CONVERS MANAGE. 2019;199:112027.

42. Laboratory NRE. Hybrid Optimization Model for Electric Renewables. 2004. p.